Multimode resonances, intermode bound states, and bound states in the continuum in waveguides

N. M. Shubin, V. V. Kapaev, and A. A. Gorbatsevich
P.N. Lebedev Physical Institute of the Russian Academy of Sciences, 119991 Moscow, Russia

(Received 20 July 2022; revised 8 September 2022; accepted 16 September 2022; published 29 September 2022)

We study analytically and numerically the formation of bound states in the continuum (BICs) in quantum-mechanical and optical spatially symmetric multimode waveguide systems. The widely used Friedrich-Wintgen model predicts a BIC for two (nearly) degenerate eigenstates of the resonator. However, numerical calculations typically show that BICs may appear away from the degeneracy point (or avoided crossing region) in the energy-parameter space. From the two-mode point of view based on the Friedrich-Wintgen model, such BICs can be considered as accidental. In this paper, we go beyond the two-mode approximation and, appealing to the notion of intermode bound states, provide an illustrative procedure for deriving conditions for BIC formation within an arbitrary finite-mode approximation. In particular, we show that a three-mode approximation allows the description of a continuous transition of a BIC between different pairs of modes, which can be associated with it within the two-mode model. Also, a manifestation of exceptional points as (anti)resonance coalescence is discussed. Analytical conclusions are verified by the results of numerical simulations of two-dimensional quantum-mechanical and optical stubbed waveguides with confining impurities in the stub. Moreover, numerical simulations confirm the existence of BICs in optical subwavelength resonators, which were earlier predicted in quantum-mechanical waveguides.

DOI: 10.1103/PhysRevB.106.125425

I. INTRODUCTION

A bound state in the continuum (BIC) is a localized state with energy embedded into the continuum of delocalized states. A BIC was first described long ago in quantum mechanics as a purely mathematical construct [1]. However, in the past years a number of realistic physical mechanisms have been proposed for how to create states with zero coupling to the continuum, and BICs have become a hot topic in physics [2–6]. Decoupling from the continuum can occur either because of different symmetry properties of the BIC and the continuum or due to the destructive interference irrespective of symmetry [2,7]. The latter implies that a BIC cannot be found in a strictly one-dimensional topologically trivial structure [6]. BICs were theoretically and experimentally studied in numerous physical systems: quantum-mechanical [7–10] and optical [11,12] waveguides (WGs), photonic crystals [13–15], subwavelength gratings [16–18], metasurfaces [19,20], acoustic resonators [21–24], etc.

An electronic conductor can be considered as a typical example of a quantum-mechanical WG. However, interelectron interactions, which are essential in electronic systems [25–29], modify BIC formation conditions and provide the possibility for new BICs to appear due to Coulomb repulsion. Recently, BIC existence was theoretically predicted and confirmed by *ab initio* simulations with at least partial accounting for Coulomb effects in molecular conductors, in particular, in such a well-studied molecule as benzene [30].

Practically, conditions for BIC formation can be most effectively realized in photonic systems [3–5], where they can be used, e.g., for the implementation of electromagnetic storage [5]. A BIC can exist only in a spatially infinite system if it is composed of materials with finite and nonzero refractive indices [31]. In a finite-size system, a BIC typically turns into a quasi-BIC possessing an extremely narrow resonance width and a high Q factor with great prospects for practical utilization [32,33].

A universal approach for BIC description [2,6] is based on the formalism of the Feshbach effective non-Hermitian Hamiltonian [34,35] with its complex eigenvalues determining poles of the scattering S matrix [36]. In this notion, BICs correspond to real eigenvalues of the effective Hamiltonian [2,6]. Therefore a BIC can be considered as a resonance of zero width [6,37]. On the other hand, the S matrix must remain finite everywhere on the real energy axis, and hence the BIC point is a point where S-matrix pole and zero must coincide [27,37,38]. Thus a BIC can be equivalently treated as an antiresonance (S-matrix zero) of vanishing width [38].

Except for those corresponding to BICs, other eigenvalues of the Feshbach effective Hamiltonian are complex due to its non-Hermiticity. However, there exists a class of non-Hermitian Hamiltonians possessing real eigenvalues—pseudo-Hermitian Hamiltonians [39,40] with $\mathcal{PT}$-symmetric Hamiltonians [41,42] being the most practically important subclass among them (here $\mathcal{P}$ and $\mathcal{T}$ stand for operations of spatial and time-reversal symmetry, correspondingly). Two real eigenvalues of a $\mathcal{PT}$-symmetric Hamiltonian can coalesce at some point of the parameter space and turn into a pair of complex-conjugate ones ($\mathcal{PT}$-symmetry breaking) [42]. Such points are called exceptional points (EPs), and they are well known from linear algebra theory [43]. In contrast to the crossing (diabolic) point, which is typical for Hermitian

operators, and where eigenstates, being degenerate, remain orthogonal, the EP provides the coalescence of two orthogonal eigenstates into a single nondegenerate one. A small perturbation, which slightly shifts a system from its EP, provides a strong nonanalytical change in its energy spectrum and properties. Therefore, at present, EPs are widely discussed in different physical systems in terms of improving sensor characteristics [44–46].

In Refs. [38,47] a representation of the transmission coefficient was proposed which relates transmission unity peaks (resonances) in a spatially symmetric system to real eigenvalues of some auxiliary $\mathcal{PT}$-symmetric Hamiltonian, which can be directly deduced from the Feshbach effective Hamiltonian. In this approach, the EP of the auxiliary Hamiltonian corresponds to the coalescence of resonances (CR) [38,48], which was recently experimentally demonstrated also in acoustic waveguides [49]. Coalescence of antiresonances (CA) can take place as well [30,38], and a mathematical description based on EPs can be applied in this case also. It is important to note that the description of such EPs is out of the scope of the traditional approach based on consideration of S-matrix poles. This is because the resonance position on the real energy (frequency) axis coincides with the real part of the S-matrix pole (Feshbach effective Hamiltonian eigenvalue) only in the case of narrow and isolated resonances [38,50].

Methods for BIC description based on the Feshbach Hamiltonian in quantum-mechanical or electromagnetic WGs usually imply a separation of the system into a cavity, the eigenstates of which determine the Hermitian part of the Feshbach Hamiltonian [6], and attached (input-output) WGs with a continuum of propagating modes (open channels) and evanescent modes in closed channels. In particular, the Friedrich-Wintgen (FW) interference mechanism of BIC formation [51] corresponds to the crossing (degeneracy) point or region of the avoided crossing of two eigenstates of the cavity and can be effectively described by a 2×2 non-Hermitian Hamiltonian [2,6]. However, separation into a cavity and attached WGs is not straightforward [52], especially for systems where eigenstates of the scattering region are strongly hybridized with WG modes, e.g., in a straight WG with impurity [8,9,53]. In this case, it seems more appropriate to utilize an approach based on the coupled-wave theory (CWT), which was initially developed for the description of distributed-feedback lasers [54,55] and later was successfully applied to the study of BICs in quantum-mechanical WGs with impurities [8,9] and photonic crystal slabs [56–58]. In Ref. [8], it was found that the BIC formation condition in a WG with impurity can be formulated in terms of two bound states (similarly to the FW model). One is an ordinary bound state split from a given mode by attractive impurity potential forming a well, which is also responsible for Fano resonance [59]. The other bound state involved is quite different and is formed in a composite quantum well due to intermode interference and nonzero intermode coupling: Well and barrier potentials are determined by the thresholds of different modes. Such a BIC typically can be described in a two-mode approximation [15]. Another example is a photonic crystal slab, where recent numerical multimode simulations [60] indicate that the main contribution to the BIC state is provided by a couple of modes. However, recently it was shown in Ref. [61] that a two-mode approximation is unable to describe, e.g., a BIC in the quantum-mechanical waveguide with a subwavelength resonator, whereas the three-mode model works well. These results demonstrate that finite-mode (i.e., two- or three-mode) approximate models within the framework of CWT can provide a sufficient background for studying complicated properties of WGs.

In this paper, we show that this is indeed the case, and via compact two- and three-mode analytical models we describe a variety of multimode interference phenomena in WGs including BICs, EPs for both resonances, and antiresonances and continuous transition between different intermode interference BICs. The latter is of special importance as it extends the FW mechanism and provides an analytical description of BICs, which cannot be described by a two-mode FW model. We refer to such BICs as "accidental" by analogy with BICs that are not symmetry protected [6,62–64]. The universality of analytic results is confirmed by multimode numerical simulations of both quantum-mechanical and electromagnetic systems.

The structure of this paper is as follows. In Sec. II we present the basic quantum-mechanical model and discuss the numerical study of a prime example of BIC formation in a WG with a stub, which by variation of the ratio of the stub to WG widths provides a BIC formation study from the case of an almost isolated cavity to the case of an almost straight multimode WG. In Sec. III some finite-mode analytical models of BIC formation and CA-CR phenomena are considered in detail based on the notion of intermode states. The continuous BIC transition between two FW-like regimes is presented and explained within the three-level model in Sec. IV. Analytical results are confirmed therein by numerical simulations. We show that such a transition can be described either on the basis of the three-mode approximation or within the three-level effective Hamiltonian model. The former approach provides a better agreement with exact results as it naturally accounts for evanescent modes in WGs. We also demonstrate numerical simulation results that confirm the existence of BICs in electromagnetic WGs with a subwavelength resonator. A discussion of the results and a conclusion are presented in Sec. V.

II. QUANTUM-MECHANICAL MULTIMODE SCATTERING PROBLEM

A. Basic equations and boundary conditions

Consider a two-dimensional (2D) system composed of a resonator attached to two WGs located along the x axis. Assuming $U(x, y)$ to be the potential profile of the whole system, one gets the following 2D Schrödinger equation:

$$\frac{\partial^2 \Psi}{\partial x^2} + \frac{\partial^2 \Psi}{\partial y^2} + [E - U(x, y)]\Psi = 0 \tag{1}$$

with appropriate boundary conditions on $\Psi(x, y)$ for either a scattering or eigenvalue problem. Here, we assume that the mass of the particle is constant over all of the system, and the units are chosen such that $\frac{\hbar^2}{2m} = 1$. We focus on the situation where $U(x, y)$ is a piecewise constant function of x, i.e., $U(x, y) = U_j(y)$ for $x_{j-1} < x \leqslant x_j$, where j enumerates

the regions. If the number of regions is M, then $x_0 = -\infty$, $x_M = \infty$, and x_1 and x_{M-1} define left and right WG-resonator interface positions, respectively.

Transverse mode decomposition [65–68] is an exact and effective way to solve Eq. (1). The general solution in the jth region can be written as follows:

$$\Psi_j(x, y) = \sum_m \psi_m^j(x) Y_m^j(y), \tag{2}$$

where $\psi_m^j(x) = A_m^j e^{ik_m^j x} + B_m^j e^{-ik_m^j x}$ with wave vector $k_m^j = \sqrt{E - \gamma_m^j}$. Transverse wave functions $Y_m^j(y)$ and corresponding eigenvalues (mode thresholds) γ_m^j are found from the 1D Schrödinger equation:

$$\frac{d^2 Y^j}{dy^2} + [\gamma^j - U_j(y)] Y^j = 0. \tag{3}$$

Summation in Eq. (2) is performed over all of the infinite number of transverse modes in the jth region (including both discrete and continuous spectra).

The scattering problem is solved via the standard transfer-matrix technique by matching wave functions (2) and their derivatives at the borders and fulfilling the appropriate boundary conditions at infinity [68]. Functions Y_m^j form an orthonormal basis set within the jth region, and hence one can formulate the continuity condition of the full wave function and its derivative between the jth and the $(j+1)$th regions as

$$\begin{aligned} \psi_n^{j+1}(x_j) &= \sum_m (\hat{\mu}_j)_{mn} \psi_m^j(x_j), \\ \frac{\partial \psi_n^{j+1}(x_j)}{\partial x} &= \sum_m (\hat{\mu}_j)_{mn} \frac{\partial \psi_m^j(x_j)}{\partial x}. \end{aligned} \tag{4}$$

Here, we have introduced a unitary infinite-dimensional transformation matrix $\hat{\mu}_j$ between basis sets $\{Y_m^j\}$ and $\{Y_m^{j+1}\}$ with elements

$$(\hat{\mu}_j)_{mn} = \int_{-\infty}^{\infty} Y_m^j(y) \left[Y_n^{j+1}(y)\right]^* dy. \tag{5}$$

Matrix $\hat{\mu}_j$ describes the mode mixing on the jth border. Equations (4) are almost identical to CWT-based equations in 2D quantum-mechanical [8] and 2D periodic photonic systems [60]. Moreover, they are quite similar to corresponding equations for 3D periodic photonic systems [58].

B. Almost isolated cavity versus almost straight multimode waveguide

As a prime example, we consider a 2D quantum-mechanical stubbed WG of width h with a stub (resonator) of width H (see inset in Fig. 1). Varying the ratio h/H from 0 to 1, one can provide a continuous transition from an almost isolated cavity to an almost straight multimode WG and study BIC formation conditions accordingly.

To be specific, we focus on the following particular electronic WG structure. Inside the WG the potential energy is set to zero, and outside the WG it is set to $U_0 = 1$ eV. The electron effective mass is assumed to be $0.0665 m_0$. To simulate states of the continuous spectra, which are needed for a proper summation in Eq. (2), we use a dense set of discrete

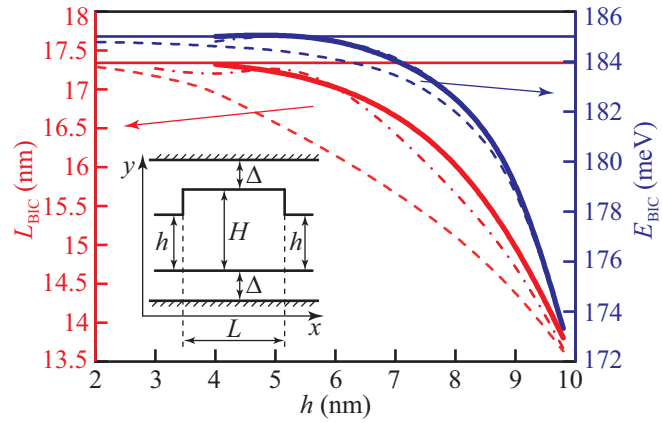

FIG. 1. Dependence of the BIC energy $E_{\rm BIC}$ and corresponding resonator's length $L_{\rm BIC}$ on the width of the attached WGs, h. Resonator width H is set to $H = 10$ nm. Thick solid lines show the exact numerical solution, and thin solid lines show the estimation for an isolated resonator (energy and condition for a pair of degenerate eigenstates). Dashed and dot-dashed lines correspond to two- and three-mode approximations. The exact numerical solution for BIC energy and the three-mode approximation almost coincide. Inset: scheme of the 2D stubbed WG structure.

transverse modes formed between artificial infinite potential borders located at some distance Δ from the structure (see inset in Fig. 1). The true continuous spectrum corresponds to $\Delta \to \infty$. Nevertheless, finite Δ can be used as long as convergence conditions are fulfilled. In the particular system considered, we set $\Delta = 10$ nm, which provides convergence with about 20–30 transverse modes taken into account, and the results demonstrate almost no dependence on Δ for $\Delta > 10$ nm [69]. Such boundary conditions seem natural for finding transverse mode eigenstates of a solitary (along the y axis) system. If the system is periodic, then Bloch wave decomposition is surely preferable [58,60].

The formation of BICs in symmetric quantum billiards due to the FW mechanism is a well-known phenomenon [7,10]. Within the effective Hamiltonian formalism for $h/H \ll 1$, one expects BICs near the degeneracy point of the isolated resonator cavity eigenstates of the same parity (with respect to mirror reflection $x \mapsto -x$). Figure 1 depicts this estimation as two horizontal lines corresponding to the energy and the resonator length providing the degeneracy of the (1,2) and (3,1) eigenstates of the isolated resonator ($h = 0$) [70]. As one can see, this estimation works pretty well for $h/H \lesssim 0.6$, whereas for wider WGs the deviation of the exact values of $E_{\rm BIC}$ and $L_{\rm BIC}$ shown by the thick solid lines becomes significant. Finally, for $h \approx H$, approximation by isolated-cavity eigenstates has nothing to do with exact BIC parameters, because splitting the system into a cavity and WGs becomes ambiguous with ill-defined eigenstates dependent on particular cavity-WG boundary conditions [52].

Fully multimode CWT calculations can be performed only numerically even for such simple geometries of the system, because dozens of transverse modes need to be taken into account for convergence. In contrast, the effective Hamiltonian formalism provides a relatively simple analysis, which has a clear physical interpretation. Thus a finite-mode ap-

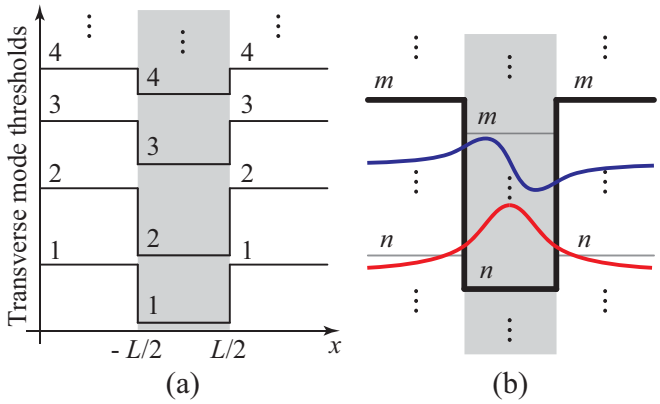

FIG. 2. (a) Energy diagram of a finite-mode quantum conductor. Thin solid lines show the mode thresholds (transverse quantization energies) in each region. The confinement region $x \in [-L/2, L/2]$ is shaded. (b) Schemes of symmetric (red) and antisymmetric (blue) intermode bound states m-n-m.

proximation in CWT with a reasonable number of transverse modes taken into account, which can be easily interpreted on the one hand, and is accurate enough on the other, is highly desirable. Analytical and numerical results of Refs. [15,60,61] suggest that two- or three-mode approximations can capture the essence of BIC formation due to multimode interference. In the rest of this paper we prove this for a wider set of physical phenomena in a particular class of the WG systems.

III. ANALYTICAL FINITE-MODE PERSPECTIVE

A. Bound states in the continuum

Consider a symmetric (with respect to the reflection $x \mapsto -x$) system consisting of three regions with borders at $x_1 = -L/2$ and $x_2 = L/2$ [Fig. 2(a)]. In this case, due to the symmetry one can denote $\hat{\mu}_1 = \hat{\mu}_2^\dagger = \hat{\mu}$. Within the finite-mode approximation, we take an arbitrary number of modes N into account in both the central confinement region (the resonator cavity) and the WGs. For definiteness, we will consider the first N modes with the lowest thresholds. However, this is not obligatory, and one can choose any N modes suitable for the particular problem. Hereinafter we assume the energy range of interest to be between the thresholds of the first and second modes in WGs. Thus the only propagating mode is the first one in each WG.

The general solution for an N-mode scattering problem is quite cumbersome and is difficult to analyze in any illustrative manner. Nevertheless, BIC formation conditions can be deduced straightforwardly. Indeed, a BIC can be found as an eigenstate with zero amplitude in the first (propagating) mode in WGs. The system under consideration is symmetric, and hence its eigenstates (including BICs) can be classified by parity as symmetric (s) and antisymmetric (a). The BIC wave function in WGs (regions 1 and 3) has the following form:

$$\psi_n^{s,a;1}(x) = a_n^{s,a} e^{\kappa_n x}, \quad \psi_n^{s,a;3}(x) = \sigma_{s,a} a_n^{s,a} e^{-\kappa_n x} \tag{6}$$

for $1 < n \leqslant N$ and $\psi_1^{s,a;1}(x) = \psi_1^{s,a;3}(x) \equiv 0$. Here, $\sigma_s = -\sigma_a = 1$ and $\kappa_n = \sqrt{\gamma_n^{1,3} - E}$ with $\gamma_n^1 = \gamma_n^3$ being the thresholds of the nth transverse mode in WGs. In the central confinement region (region 2), the wave functions of the symmetric and antisymmetric BICs are as follows:

$$\psi_n^{s,2}(x) = b_n^s \cos k_n x, \quad \psi_n^{a,2}(x) = b_n^a \sin k_n x. \tag{7}$$

Here, $k_n = \sqrt{E - \gamma_n^2}$, and γ_n^2 is the threshold of the nth transverse mode in the cavity.

Applying boundary conditions (4) to the wave functions (6) and (7), one gets a homogeneous system of $2N$ linear equations for $2N-1$ variables $\{a_2^s, a_3^s, \ldots, a_N^s, b_1^s, b_2^s, \ldots, b_N^s\}$, which defines symmetric BICs, and another homogeneous system of $2N$ linear equations for $2N-1$ variables $\{a_2^a, a_3^a, \ldots, a_N^a, b_1^a, b_2^a, \ldots, b_N^a\}$, which defines antisymmetric BICs. In order to have nontrivial solutions for these systems, any $2N-1$ equations in them must be linearly dependent. After some algebra [69], one gets that this requirement can be formulated as a condition of simultaneous vanishing of all minors $\Delta_{n,1}^{s,a}$ of the matrices $\hat{M}^{s,a}$ for any $1 \leqslant n \leqslant N$. Matrices $\hat{M}^{s,a}$ here are given by $(\hat{M}^{s,a})_{nm} = \mu_{mn} A_{mnm}^{s,a}$, where

$$\begin{aligned} A_{mnm}^s &= k_n \sin\left(\frac{k_n L}{2}\right) - \kappa_m \cos\left(\frac{k_n L}{2}\right), \\ A_{mnm}^a &= \kappa_m \sin\left(\frac{k_n L}{2}\right) + k_n \cos\left(\frac{k_n L}{2}\right). \end{aligned} \tag{8}$$

The physical meaning of quantities $A_{mnm}^{s,a}$ is quite clear because condition $A_{mnm}^{s,a} = 0$ defines an intermode state m-n-m, which is localized at the mth transverse mode in WGs and at the nth mode in the resonator [see Fig. 2(b) for an illustration] [61]. Obviously, condition $A_{nnn}^{s,a} = 0$ describes an ordinary symmetric or antisymmetric state in a quantum well within the nth mode. For more definiteness, hereinafter m-n_y-$m(n_x)$ will refer to intermode states which tend to (n_x, n_y) in the limit of an isolated resonator.

One can reduce the requirement of $\Delta_{n,1}^{s,a} = 0$ for all $1 \leqslant n \leqslant N$ to only the following pairs of equations for any n and $m \neq n$ [69]:

$$\begin{cases} \Delta_{n,1}^s = 0 \\ \Delta_{m,1}^s = 0 \end{cases} \quad \text{or} \quad \begin{cases} \Delta_{n,1}^a = 0 \\ \Delta_{m,1}^a = 0. \end{cases} \tag{9}$$

Thus there are $N(N-1)/2$ possible pairs of BIC condition equations, which are all equivalent. One can see from Eqs. (9) that conditions for BIC formation, which take into account N transverse modes, can be reduced to the conditions involving $N-1$ modes, if corresponding mode-mixing matrix elements μ_{nN} and μ_{Nn} are negligible for $1 \leqslant n < N$. Thus a thorough preliminary analysis of the mode-mixing matrix should be performed before making a decision on which finite-mode approximation is suitable in each particular system.

As an example, let us consider the simplest multimode model with $N = 2$ and some more general cases with $N > 2$. For $N = 2$, conditions (9) turn into

$$\begin{aligned} A_{222}^{s,a} &= 0 \\ A_{212}^{s,a} &= 0. \end{aligned} \tag{10}$$

These conditions are exactly the same as those that were first derived in Ref. [8] and require the degeneracy of 2-2-2 and 2-1-2 intermode localized states of the same parity. It should be noted that conditions (10) do not depend on the

mode-mixing matrix $\hat{\mu}$. Two-mode approximation [for states 2-2-2(1) and 2-1-2(3)] provides a better agreement with exact BIC parameters in the example shown in Fig. 1 than isolated resonator estimation.

A substantially different situation takes place for $N = 3$, in which case BIC conditions become [one of $N(N-1)/2 = 3$ equivalent formulations]

$$\begin{aligned} \mu_{21}\mu_{33}A^{s,a}_{212}A^{s,a}_{333} - \mu_{31}\mu_{23}A^{s,a}_{232}A^{s,a}_{313} = 0 \\ \mu_{22}\mu_{33}A^{s,a}_{222}A^{s,a}_{333} - \mu_{23}\mu_{32}A^{s,a}_{232}A^{s,a}_{323} = 0. \end{aligned} \tag{11}$$

Here, dependence on mode-mixing matrix $\hat{\mu}$ is essential. Three-mode approximation gives even better agreement with exact BIC parameters in the example structure considered in Fig. 1.

It seems that conditions (11) can be fulfilled if $A^{s,a}_{333} = A^{s,a}_{232} = 0$, i.e., if intermode localized states 3-3-3 and 2-3-2 of the same parity are degenerate. However, this is not possible because bound state energies in quantum wells, which differ only by barrier height, cannot coincide. Conditions (11) show that a BIC can be formed in the case of triple degeneracy of intermode states 2-1-2, 2-2-2, and 2-3-2 or intermode states 3-1-3, 3-2-3, and 3-3-3. Surely, this requirement is much more difficult to fulfill compared with two-mode degeneracy (10). In contrast to the two-mode case, in the three-mode approximation, a new type of BIC can arise with none of $A^{s,a}_{mnm}$ turning to zero, which indicates a truly multimode interference.

Finite-mode approximations with $N > 3$ become much more complicated but still can be more or less illustratively interpreted and analyzed. See the Appendix for an example with $N = 4$. Multimode consideration allows the generalization of the two-mode BIC conditions to the requirement of degeneracy between any two intermode bound states *m-n-m* and *p-q-p*,

$$A^{s,a}_{mnm} = A^{s,a}_{pqp} = 0, \tag{12}$$

if the corresponding matrix elements μ_{mn} and μ_{pq} are dominant. Surely, here we do not consider $m = 1$ or $p = 1$ because in that case corresponding intermode states would not be bound within the energy range of interest.

B. Two-mode model: Bound states in the continuum and exceptional points

Within the two-mode approximation, we account only for two modes of transverse quantization in each region. For brevity, we assume $\gamma^1_1 = \gamma^3_1 = U_1$ and $\gamma^1_2 = \gamma^3_2 = U_2$ as thresholds of the first and the second modes in the attached WGs and $\gamma^2_1 = V_1 \leqslant U_1$ and $\gamma^2_2 = V_2 \leqslant U_2$ as thresholds inside the confinement region (resonator cavity).

Straightforwardly discarding all other mode-mixing matrix elements except for those corresponding to two selected modes leads to the inconsistency of the solution due to the fact that matrix $\hat{\mu}$ becomes nonunitary and hence does not preserve particle and current conservation. Thus, within our illustrative consideration of a simplified two-mode model, we assume the 2×2 matrix $\hat{\mu}$ to be unitary. Without loss of generality, any 2×2 unitary matrix can be written in the Euler angle parametrization [71] as

$$\hat{\mu} = \begin{pmatrix} e^{i\varphi_1}\cos\theta & e^{i\varphi_2}\sin\theta \\ -e^{i(\varphi-\varphi_2)}\sin\theta & e^{i(\varphi-\varphi_1)}\cos\theta \end{pmatrix} \tag{13}$$

with $\theta, \varphi, \varphi_1, \varphi_2 \in \mathbb{R}$. In fact, in the considered WG systems, transverse wave functions are real valued, and hence φ, φ_1, and φ_2 turn out to be either zero or π. Parameter θ indicates the "strength" of the mode mixing, e.g., for the $\theta = 0$ matrix, $\hat{\mu}$ is diagonal and modes are fully independent, whereas for $\theta = \frac{\pi}{2}$, modes totally interchange on each border.

Within the two-mode approximation, the full scattering problem can be solved, and various interference phenomena can be analyzed. Consider an incident particle with energy $U_1 < E < U_2$ in the first mode going from the left. Using wave-function matching (4) and the definition (13), one can derive the transmission coefficient of the system (from the first mode in the left WG to the first mode in the right WG) in the general form [38,72]

$$T(E) = \frac{|P(E)|^2}{|P(E)|^2 + |Q(E)|^2}, \tag{14}$$

with

$$\begin{aligned} P(E) &= 2k\left[k_1 A^s_{222}A^a_{222}\cos^2\theta + k_2 A^s_{212}A^a_{212}\sin^2\theta\right], \\ Q(E) &= V_1 A^s_{222}A^a_{222}\sin(k_1 L)\cos^4\theta + V_2 A^s_{212}A^a_{212}\sin(k_2 L)\sin^4\theta + 2\cos^2\theta\sin^2\theta \\ &\quad\times\left\{A^a_{212}A^s_{222}\left[k^2\sin\left(\frac{k_2 L}{2}\right)\cos\left(\frac{k_1 L}{2}\right) - k_1 k_2\sin\left(\frac{k_1 L}{2}\right)\cos\left(\frac{k_2 L}{2}\right)\right]\right. \\ &\quad\left. + A^s_{212}A^a_{222}\left[k^2\sin\left(\frac{k_1 L}{2}\right)\cos\left(\frac{k_2 L}{2}\right) - k_1 k_2\sin\left(\frac{k_2 L}{2}\right)\cos\left(\frac{k_1 L}{2}\right)\right]\right\}. \end{aligned} \tag{15}$$

We have introduced here $k = \sqrt{E - U_1}$, $k_{1,2} = \sqrt{E - V_{1,2}}$, and $\kappa = \sqrt{U_2 - E}$, and $A^{s,a}_{mnm}$ are given by Eqs. (8). From the general equations (15), one can easily derive $P(E)$ and $Q(E)$ functions in limiting cases of independent modes ($\theta = 0$) and fully interchange modes on each border ($\theta = \pi/2$):

$$P_0(E) = 2kk_1 A^s_{222}A^a_{222}, \quad Q_0(E) = V_1 A^s_{222}A^a_{222}\sin(k_1 L) \tag{16}$$

and

$$P_{\frac{\pi}{2}}(E) = 2kk_2 A^s_{212}A^a_{212}, \quad Q_{\frac{\pi}{2}}(E) = V_2 A^s_{212}A^a_{212}\sin(k_2 L). \tag{17}$$

For $\theta = 0$, electrons go through the first mode only, and resonant transmission takes place at $k_1 L = \pi n$, $n \in \mathbb{Z}$, where Q_0 becomes zero. At the same time, the second mode appears to be completely decoupled from the transport process, and hence localized states in the second mode, which we refer to as 2-2-2, turn into BICs [73]. Indeed, as one can see from Eqs. (16), condition $A^{s,a}_{222} = 0$ defining the symmetric and antisymmetric bound states in the second mode, respectively, provides $Q_0 = 0$ and $P_0 = 0$ simultaneously, which indicates BIC formation [38].

For $\theta = \frac{\pi}{2}$, electrons from the first mode go through the second mode in the confinement region and then go away in the first mode again. In this case, resonant transmission takes place at $k_2 L = \pi n$, $n \in \mathbb{Z}$, where $Q_{\frac{\pi}{2}}$ turns to zero. Similar to the $\theta = 0$ case, there are fully localized states (BICs) with energies defined by the condition $A^{s,a}_{212} = 0$. These states are localized in the first mode of the confinement region and decay into the second mode outside the central region, and hence we call them 2-1-2.

The abovementioned states take place only in two mutually exclusive limiting cases of parameter θ. Nevertheless, according to the general formulas (14) and (15) they determine the behavior of the transmission coefficient for arbitrary θ. Zeros of function $P(E)$ correspond to energies of perfect reflection, and zeros of function $Q(E)$ correspond to energies of perfect transmission. Exact analysis of expressions (15) is difficult; however, some striking features can be easily determined. Indeed, function $P(E)$ becomes zero if either $A^{a,s}_{212} = A^{s,a}_{222} = 0$ or $A^{s,a}_{212} = A^{s,a}_{222} = 0$. In the former case, function $Q(E)$ is strictly nonzero, which means that condition $A^{a,s}_{212} = A^{s,a}_{222} = 0$ defines the transmission dip (antiresonance), whereas in the latter case function $Q(E)$ becomes zero as well. Hence the condition $A^{s,a}_{212} = A^{s,a}_{222} = 0$ indicates the formation of a BIC [38]. In other words, degeneracy of bound states 2-2-2 and 2-1-2 of the same parity (both either symmetric or antisymmetric) provides the formation of a BIC that fully agrees with condition (10). The analysis performed above shows that intermode states located in different modes (2-1-2) are involved in the buildup of transmission resonances and antiresonances and BIC formation on an equal basis with ordinary states localized in a single mode (2-2-2).

EPs in the transmission spectrum manifest themselves as a coalescence of either resonances [38,48,49] or antiresonances [30]. In the energy-parameter space, such points can be identified as points, where tangent line to the perfect resonance (antiresonance) curve becomes parallel to the energy axis. Consider in more detail the case of two degenerate states 2-2-2 and 2-1-2 of different parity with energy E_0. Then, the condition $A^{a,s}_{212} = A^{s,a}_{222} = 0$ will be fulfilled at $E = E_0$ leading to $P(E_0) = 0$, $Q(E_0) \neq 0$, and consequently $T(E_0) = 0$. Moreover, thorough analysis of formulas (15) shows that, similarly to the molecular conductors with degenerate orbitals of different parity [30], the second-order multiple root of $P(E)$ and CA can be achieved exactly at energy E_0 if $\theta = \arctan[\sqrt{\frac{(E_0 - V_1)(U_2 - V_2)}{(E_0 - V_2)(U_2 - V_1)}}]$. In the general case of arbitrary θ, however, CA does not take place exactly at the point in the energy-parameter space given by the condition $A^{a,s}_{212} = A^{s,a}_{222} = 0$, but in some vicinity of it.

In Ref. [74], it was shown that CR can also take place in the vicinity of two degenerate states of opposite parity. However, it cannot be explicitly identified as an EP of some auxiliary Hamiltonian because the latter is not defined within the CWT formalism. Nevertheless, CR can be recognized from the direct analysis of $Q(E)$ given by Eq. (15). One of the striking features of an operator near an EP is the nonanalytical behavior of its eigenvalues [45]. In particular, in the case of a second-order EP, splitting between the eigenvalues is proportional to the square root of perturbation. As we demonstrate in the example below in the present section, this is exactly the case for CR and CA phenomena.

As an illustration let us consider the system with $U_1 = 0$, $U_2 = 10$, $V_1 = -2$, and $V_2 = 5$. Using Eqs. (14) and (15), one can calculate the energy-resolved transmission spectrum for different values of the central region length L. Density plots of the calculated transmission coefficient are shown in Fig. 3 with different values of θ. For small θ [Fig. 3(a)] the contribution of the first term in the expression (15) for $P(E)$ is dominant, and hence transmission dips follow predominantly zeros of $A^{s,a}_{222}$ (i.e., bound states of 2-2-2 type). On the other hand, if θ is close to $\frac{\pi}{2}$ [Fig. 3(b)], then the second term in the expression for $P(E)$ is dominant, and antiresonances follow zeros of $A^{s,a}_{212}$ (bound states of 2-1-2 type). In the intermediate regime [Fig. 3(c)] the behavior of resonances and antiresonances is rather complicated. As was stated above, BICs arise in the case of degeneracy between 2-2-2 and 2-1-2 states of the same parity (the intersection of dashed and solid lines of the same color in Fig. 3), and their position (energy and corresponding resonator length) does not depend on the parameter θ.

EPs associated with CA and CR are less strictly defined but typically take place in the vicinity of the degeneracy point between intermode states 2-2-2 and 2-1-2 with opposite parity [the intersection of dashed and solid lines of different color (blue and red) in Fig. 3]. As we have shown above, one can observe CA for exactly degenerate states only for some specific value of θ [as in Fig. 3(d)]. Near any CR and CA, perfect transmission resonances and zero transmission antiresonances demonstrate square-root behavior with varying L [see parabolic approximations, shown by dashed lines in the insets in Fig. 3(c)]. This is a clear manifestation of an underlying EP, which was earlier established within the tight-binding formalism [30,38].

IV. TRANSITION OF BOUND STATES IN THE CONTINUUM BETWEEN DIFFERENT TWO-MODE REGIMES

A. Quantum-mechanical waveguides

Typically, the two-mode CWT approximation (10) provides a quite accurate prediction for BIC energy and formation conditions [8,15]. As we have shown above, the multimode consideration suggests that the choice of particular transverse modes for decomposition is performed in accordance with the corresponding mode-mixing matrix elements. Thus different system parameters can provide different pairs of modes involved in BIC formation. Consequently, there might be a transition of a BIC between different pairs of modes, which it

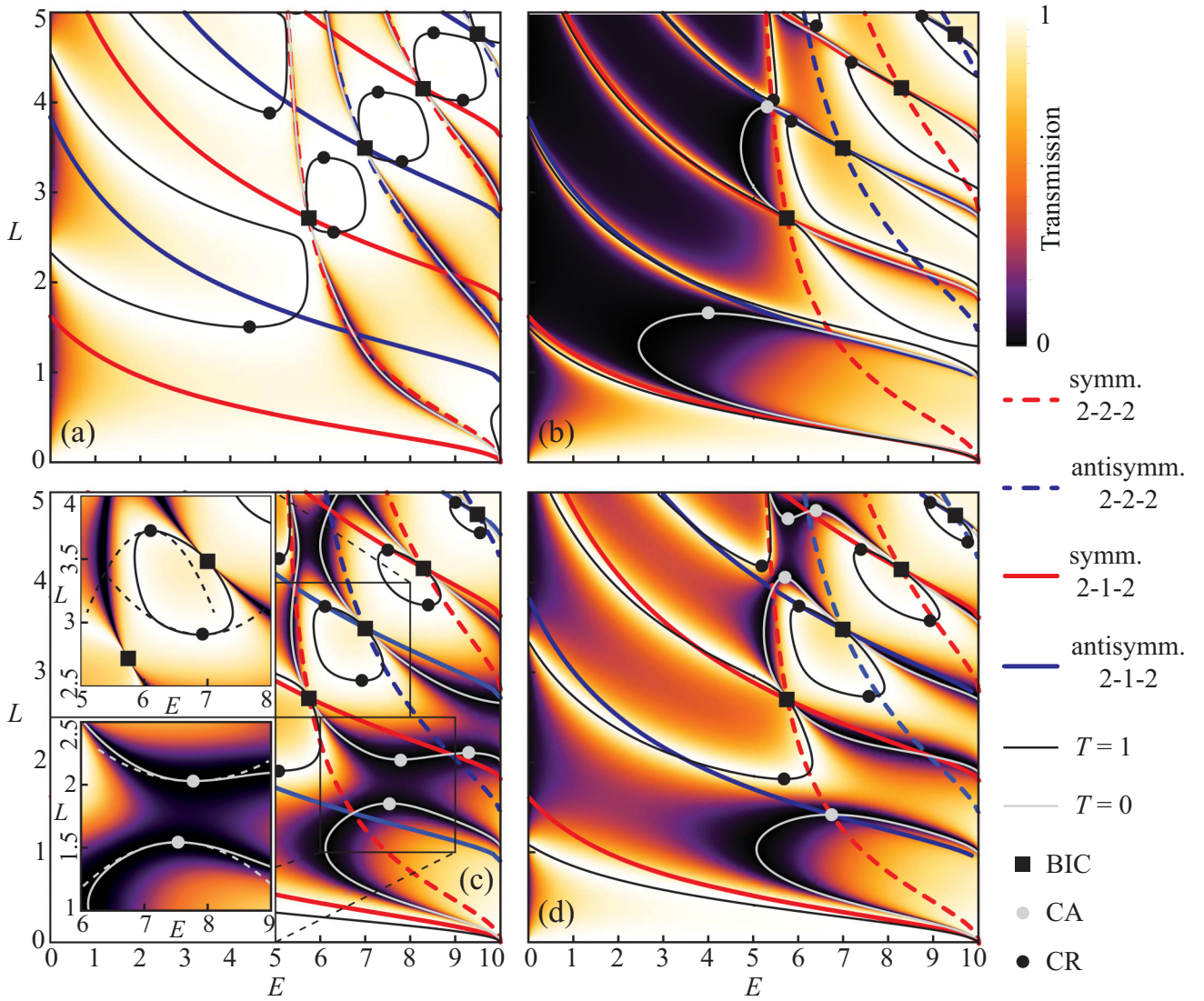

FIG. 3. Energy-vs-resonator-length diagrams of the transmission coefficient for $\theta = 0.3$ (a), $\theta = \frac{\pi}{2} - 0.3$ (b), $\theta = \frac{\pi}{4}$ (c), and $\theta = 0.967\,562$ (d). Parabolic approximations for the positions of transmission resonances or antiresonances near the CR and CA points, respectively, are depicted by dashed lines in the insets in (c). The case shown in (d) corresponds to the specific choice of θ which leads to the CA being exactly at the degenerate intermode states of different parity (at approximately $L_{\mathrm{BIC}} \approx 1.435\,703$ and $E_{\mathrm{BIC}} \approx 6.725\,358$). Here, symm., symmetric; antisymm., antisymmetric.

can be associated with. Without going beyond the two-mode approximation [even in its generalized version (12)], BICs in such a transition might be thought of as accidental.

As a quantum-mechanical model for numerical simulations, we consider a symmetric 2D stubbed WG structure. Inside the electron WG, we set the potential energy to zero, and outside it, we set the potential energy to $U_0 = 1$ eV. We also consider an additional quantum well with potential U_w and width w inside the stub (see inset in Fig. 4). The structure is similar to that considered in Ref. [53], where, however, insight into the multimode BIC formation was not established. The additional quantum well allows more precise and effective control of mode-mixing matrix elements μ_{mn} as well as transverse mode thresholds, which also enter into, e.g., the condition for BIC formation (11) through quantities A_{mnm}. Thus one can write the following expression for the potential energy of the considered 2D system:

$$U(x,y) = \begin{cases} U_0, & y < 0 \\ U_w, & 0 \leqslant y < w \\ 0, & w \leqslant y < H \\ U_0, & y \geqslant H \end{cases} \tag{18}$$

for $|x| \leqslant L/2$ (inside the resonator) and

$$U(x,y) = \begin{cases} U_0, & y < 0 \\ 0, & 0 \leqslant y < h \\ U_0, & y \geqslant h \end{cases} \tag{19}$$

for $|x| > L/2$ (outside the resonator). The electron effective mass is assumed to be $0.0665 m_0$. For numerical simulation of a continuous spectrum, we again introduce artificial borders along the x axis at a distance $\Delta = 10$ nm from the resonator as discussed in Sec. II.

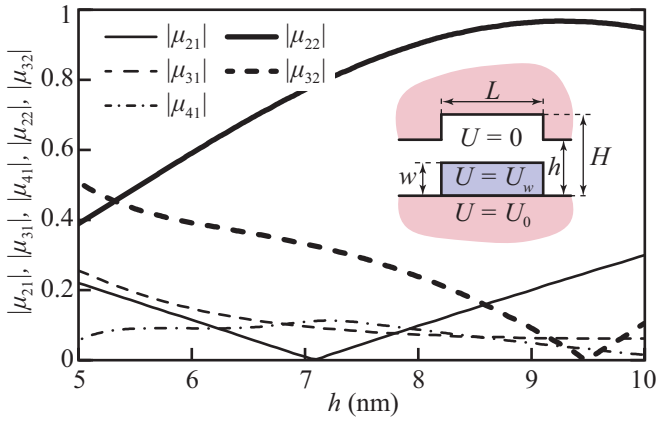

FIG. 4. Absolute value of mode-mixing matrix elements $|\mu_{21}|$, $|\mu_{31}|$, $|\mu_{41}|$, $|\mu_{22}|$, and $|\mu_{32}|$ vs h for the structure with $H = 10$ nm, $U_w = -0.1$ eV, and $w = 4$ nm. The inset depicts a scheme of the considered 2D stubbed WG with an additional quantum well in the resonator.

Preliminary two-mode consideration [in its generalized form (12)] requires analysis of mode-mixing matrix elements μ_{mn}. Figure 4 depicts the dependence of matrix elements μ_{21}, μ_{31}, μ_{41}, μ_{22}, and μ_{32} on the waveguide width h for the structure with $H = 10$ nm, $U_w = -0.1$ eV, and $w = 4$ nm. Matrix elements μ_{22} and μ_{21} are the greatest for $h \gtrsim 8$ nm, whereas μ_{32} and μ_{31} dominate for $h \lesssim 5.5$ nm ($|\mu_{22}| > |\mu_{31}|$, but states 2-2-2 and 3-2-3 cannot be degenerate and hence cannot provide a BIC). Thus, within the generalized two-mode point of view, one expects a BIC due to the interference between degenerate states 2-1-2 and 2-2-2 for $h \gtrsim 8$ nm and between 3-1-3 and 3-2-3 for $h \lesssim 5.5$ nm. That is exactly the case, as shown in Fig. 5. Indeed, for $h \gtrsim 8.5$ nm, the low-energy BIC (blue line) is well described by two-mode interference between degenerate 2-2-2(1) and 2-1-2(5) states, and the high-energy BIC (red line) is well described by two-mode interference between degenerate 2-2-2(1) and 2-1-2(3) states. For $h \lesssim 7$ nm, the low-energy BIC corresponds to degenerate 3-2-3(1) and 3-1-3(3) states. The high-energy BIC, in this case, can take place for arbitrary small resonator length (with energy tending to the threshold of the second mode in WG) and, as was shown in Ref. [61], cannot be described within the two-mode approximation. Intermediate values of h provide a continuous transition between these limiting cases, where, at first sight, BICs can be thought of as being accidental.

The first step beyond the two-mode approximation is the three-mode approximation, which provides Eqs. (11) as conditions for BIC formation. We focus on energies below states 3-3-3 and 2-3-2; so $A^{s,a}_{333}$ and $A^{s,a}_{232}$ can be considered as nonzero energy-independent quantities in the energy range of interest. The first equation in (11) is approximately satisfied by $A^{s,a}_{212} \approx 0$ if $|\mu_{21}| > |\mu_{31}|$, which is the case for $h > 8$ nm (Fig. 4), and by $A^{s,a}_{313} \approx 0$ if $|\mu_{21}| < |\mu_{31}|$, which is the case for $h < 7.5$ nm (Fig. 4). The second equation in (11) can be analyzed similarly. For $|\mu_{22}\mu_{33}| > |\mu_{32}\mu_{23}|$, that corresponds to $h > 7$ nm; it is satisfied approximately by $A^{s,a}_{222} \approx 0$, and by $A^{s,a}_{323} \approx 0$ for $|\mu_{22}\mu_{33}| < |\mu_{32}\mu_{23}|$ ($h < 6.5$ nm). Thus limiting cases are captured well by the three-mode approximation.

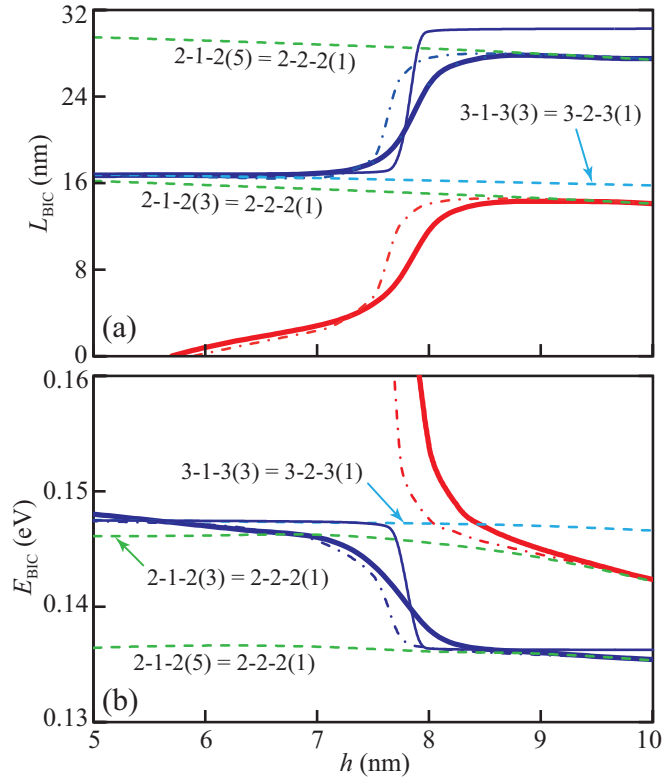

FIG. 5. Dependence of the resonator length L_{BIC} (a) and energy E_{BIC} (b) of exact BICs on the WG width h (blue and red thick solid lines) and comparison with estimation for two-mode (dashed lines) and three-mode (dot-dashed lines) approximations. The three-level effective Hamiltonian model for the low-energy BIC transition is shown by the thin solid blue lines. Parameters are set to $U_w = -0.1$ eV, $H = 10$ nm, and $w = 4$ nm. It is not shown in the scale of (b), but the energy E_{BIC} of the high-energy BIC [red line in (b)] goes up to the threshold of the second mode in WG $\gamma_2^{1,3} \approx 0.411$ eV as the corresponding resonator length L_{BIC} tends to zero at $h \approx 5.76$ nm.

Moreover, as one can see from Fig. 5 that the three-mode approximation also qualitatively reproduces the transition region. Deviation from the exact values of L_{BIC} and E_{BIC} is observed in the region around $h \sim 7.5$ nm (Fig. 5), where the matrix element μ_{41} becomes significant (Fig. 4).

B. Effective Hamiltonian model for transition of a bound state in the continuum

One can show that the above-discussed transition of a BIC is an inherent property of a three-level model with the bare Hamiltonian

$$\hat{H}_0 = \begin{pmatrix} \varepsilon_1 & \tau_1 & 0 \\ \tau_1 & \varepsilon_2 & \tau_3 \\ 0 & \tau_3 & \varepsilon_3 \end{pmatrix} \tag{20}$$

coupled to a single continuum with the coupling matrix [75] $\hat{\Gamma} = \mathbf{u}\mathbf{u}^\dagger$, where

$$\mathbf{u}^\top = (\gamma_1, \gamma_2, \gamma_3), \tag{21}$$

which is energy independent within the wide-band limit (WBL) [76]. Here, we take $\tau_{1,3}$ and $\gamma_{1,2,3}$ to be real, and for definiteness we assume that $\tau_{1,3}$ and $\gamma_{1,3}$ are positive. This

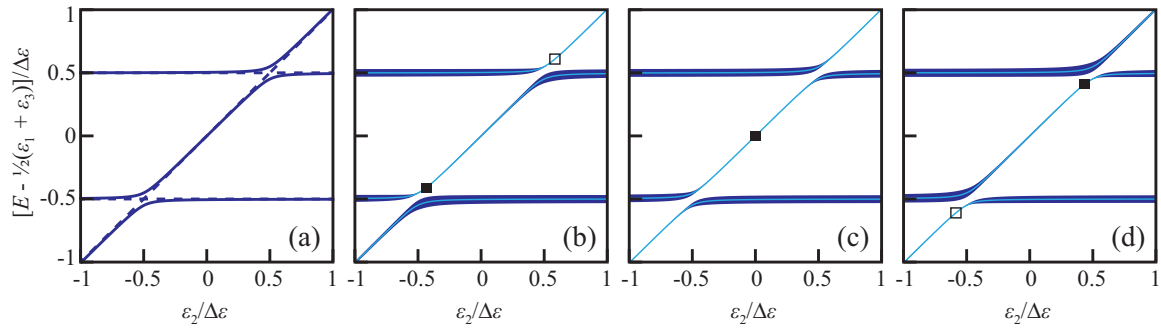

FIG. 6. (a) Energy spectrum of the three-level model for $\tau_1 = \tau_3 = 0.05\Delta\varepsilon$ (solid lines) and for $\tau_1 = \tau_3 = 0$ (dashed lines). For certainty, we assume $\varepsilon_1 > \varepsilon_3$. (b)–(d) Dependence of the real (cyan solid lines) and imaginary (blue line width) parts of the effective Hamiltonian $\hat{H}_{\text{eff}} = \hat{H}_0 - i\hat{\Gamma}$ eigenvalues for $\gamma_2 = -\frac{1}{16}\sqrt{2\Delta\varepsilon}$ (b), $\gamma_2 = 0$ (c), and $\gamma_2 = \frac{1}{16}\sqrt{2\Delta\varepsilon}$ (d), while $\gamma_1 = \gamma_3 = \frac{1}{8}\sqrt{2\Delta\varepsilon}$ are fixed. The transition of the BIC (labeled with a solid black square) from one avoided crossing region to another is clearly seen. The BIC which is not of interest as it goes to infinity for $\gamma_2 = 0$ is labeled with an open square.

three-level system can be thought of as a generalization of the Pavlov-Verevkin model [77,78], which considers N degenerate states (the bare Hamiltonian is proportional to the $N \times N$ identity matrix) coupled to K continua, to the case of nondegenerate states (for $N = 3$ and $K = 1$). BIC formation in 3D acoustic systems with $N = 3$ degenerate states coupled to $K = 2$ continua was also thoroughly studied in Refs. [79,80].

Suppose that energies ε_1 and ε_3 are fixed and ε_2 is varied. The considered model is assumed to provide physical insight into the phenomenon of continuous transition between the two FW-like BICs described in Sec. IV A. Thus we restrict it to the case $\varepsilon_1 \neq \varepsilon_3$, which gives two avoided crossing regions (for $\tau_{1,3} \neq 0$) at $\varepsilon_2 \approx \varepsilon_{1,3}$ and energy $E \approx \varepsilon_{1,3}$, respectively, as Fig. 6(a) illustrates. The limiting case $\varepsilon_1 = \varepsilon_3$ does not properly fit the purpose of the model, and hence it is out of our scope.

Following the auxiliary Hamiltonian formalism [38] [the formalism of $P(E)$ and $Q(E)$ functions], one can straightforwardly derive the energy and value of ε_2 providing the BIC formation. Surely, the same result can be obtained within the standard effective Hamiltonian approach [6,81]. However, for $N > 2$, simultaneous analysis of two real functions (P and Q) provides a rather simpler way of getting analytical conclusions compared with study of the complex eigenvalues of a non-Hermitian Hamiltonian [69].

Assuming that avoided crossing regions are small compared with the energy split between the first and the third states ($\tau_{1,3} \ll |\varepsilon_1 - \varepsilon_3|$), one can get that there are two BICs, one of which has energy between ε_1 and ε_3 for $\gamma_2 = 0$, while the other goes to infinity for $\gamma_2 \to 0$. The latter is not of interest as in real systems it would be influenced by some distant levels and hence cannot be studied within our three-level model. The energy of the former for $\gamma_2 = 0$ is

$$E_{\text{BIC}} = \frac{\varepsilon_1\eta^{-1}\tau_3 + \varepsilon_3\eta\tau_1}{\eta\tau_1 + \eta^{-1}\tau_3}, \tag{22}$$

at

$$\varepsilon_2^{\text{BIC}} = E_{\text{BIC}} + \frac{\tau_1^2 - \tau_3^2 + \tau_1\tau_3(\eta^{-2} - \eta^2)}{\Delta\varepsilon}, \tag{23}$$

where $\eta = (\gamma_1/\gamma_3)^{1/2}$ and $\Delta\varepsilon = \varepsilon_1 - \varepsilon_3$. Introduction of $\gamma_2 \neq 0$ shifts the energy of the BIC and corresponding $\varepsilon_2^{\text{BIC}}$ towards the avoided crossing region of either the first and the second states (for $\gamma_2 > 0$) or the third and the second states (for $\gamma_2 < 0$). Thus continuous transition of a BIC between two avoided crossing regions can be realized if one tunes γ_2 in a way that it changes its sign. Figure 6 illustrates this behavior.

The presented three-level model can be applied directly to the WG system considered in the previous section if one takes, e.g., eigenstates (n_x, n_y) of the isolated resonator region as initial levels and their couplings to the first propagating mode in WGs as γ_i. In accordance with Refs. [10,52], these couplings are naturally related to the mode-mixing matrix elements μ_{1n_y}. For instance, the BIC transition shown by the blue line in Fig. 5 can be qualitatively described by the model given in (20) and (21) if one relates energies of the eigenstates (5,1) and (3,1) to ε_1 and ε_3, respectively; the energy of the (1,2) state to ε_2; and matrix elements μ_{11} and μ_{12} to couplings $\gamma_1 = \gamma_3$ and γ_2, respectively. Parameter τ_1 or τ_3 can be extracted as a half of the minimal energy split within the avoided crossing region between states (5,1) and (1,2) or (3,1) and (1,2), correspondingly. While varying h from $h = 5$ nm to $h = H = 10$ nm, matrix element μ_{11} demonstrates a weak dependence on h, remaining $\mu_{11} \approx 0.95$. On the other hand, μ_{12} depends almost linearly on h and changes its sign at $h \approx 7.81$ nm. Thus one expects that the model given in (20) and (21) will describe the BIC transition for the considered WG system, which, indeed, takes place, and the result is illustrated in Fig. 5 by the thin solid blue lines.

The fact that the exact BIC beyond the transition region follows the degeneracy of intermode states [3-1-3(3) and 3-2-3(1) or 2-1-2(5) and 2-2-2(1)] instead of isolated resonator cavity eigenstates (n_x, n_y) arises due to the influence of evanescent modes in WGs. Within the effective Hamiltonian formalism, consideration of evanescent modes requires a dramatic complication of the analysis [7]. On the other hand, introduction of intermode states provides a natural way of taking evanescent modes into account, which is a key advantage for description of WG systems with strongly hybridized eigenstates of the resonator cavity.

C. Optical waveguides

A natural correspondence exists between quantum mechanics and optics [82]. Therefore one may expect a similar multimode mechanism of BIC formation to take place in optical WGs. The Helmholtz equation for the transverse electric (TE) wave in a 2D system can be written in the form (1) but for electric field distribution $E(x, y)$ instead of wave function $\Psi(x, y)$ and with refractive index $[2\pi\lambda^{-1}n(x, y)]^2$ instead of potential energy $[E - U(x, y)]$. However, in optics, there is a fundamental complication of the BIC-finding procedure compared with quantum mechanics due to the form of the Helmholtz equation, which provides the dependence of mode-mixing matrix elements μ_{mn} on the wavelength. Nevertheless, as we show below, the transition of a BIC between different pairs of intermode states due to multimode interference can also be observed in optical WGs. Moreover, the formation of a BIC in a subwavelength resonator does take place in an optical WG, similar to the quantum-mechanical case [61].

We consider the same 2D geometry of the stubbed optical WG as in the quantum-mechanical case (inset in Fig. 4). We set the refractive index to $n = 1.5$ inside the WG and $n_0 = 1$ outside it. Instead of a quantum well of depth $|U_w|$ within the stub we take an impurity with refractive index $n_w > n$. It should be noted that since there are no true bound states in 2D purely dielectric WGs [82–84], we need to confine the electromagnetic field by ideally conducting plates, located at some distance Δ from the cavity (as shown in the inset in Fig. 1 for the quantum-mechanical system). The result of numerical calculations depends strongly on Δ, but the qualitative illustration of multimode BIC formation can be performed for any value of Δ, and hence we focus on the simplest situation with $\Delta = 0$.

Analysis of mode-mixing matrix elements (for the first several transverse modes) shows that diagonal matrix elements μ_{22} and μ_{33} dominate over nondiagonal ones: $|\mu_{22}|, |\mu_{33}| \gg |\mu_{mn}|$ with $m \neq n$ due to the relatively small contrast of the refractive index. However, in the energy range of interest, corresponding states 2-2-2 and 3-3-3 cannot be degenerate as 3-3-3 states have sufficiently shorter wavelength. Thus the two-mode approximation suggests that BICs within the considered range of parameters can be described by degeneracy of the 2-2-2 state with intermode states m-1-m ($m > 1$). Figure 7 shows the dependencies of the matrix element absolute values $|\mu_{21}|$, $|\mu_{31}|$, and $|\mu_{41}|$ on the wavelength λ for different values of the impurity refractive index n_w. As in quantum-mechanical WG, $|\mu_{21}|$ typically exceeds $|\mu_{31}|$ and $|\mu_{41}|$. However, for $n_w \approx 1.85$, there is a range of wavelength around $\lambda/h \sim 4$ where μ_{21} turns to zero and μ_{31} is predominant. Therefore one may expect a BIC transition and also the possibility for BIC formation for an arbitrary small resonator length as was shown previously for quantum mechanics [61].

By varying the dielectric constant of the impurity n_w, one can see (Fig. 8) the transition of BICs between different pairs of intermode states they can be associated with within the two-mode approximation. Regardless of the fact that μ_{31} is slightly greater than μ_{21} in the considered wavelength range for $n_w \sim 1.8$ [see Fig. 7(b)], BIC follows the degeneracy of 2-1-2 and 2-2-2 states for these parameters as well as for $n_w \sim 1.85$ (Fig. 8). This can be easily understood from the

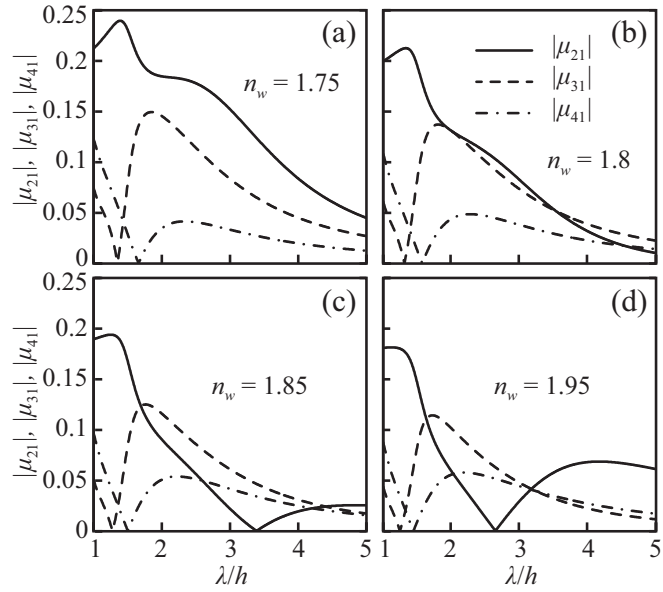

FIG. 7. (a)–(d) Dependence of the absolute value of matrix elements $|\mu_{21}|$, $|\mu_{31}|$, and $|\mu_{41}|$ on the wavelength λ for impurity with $w = 1.2h$ width and different refractive indices. The stub width is set to $H = 3h$.

three-mode approximation (11), which works for this example even better than in the quantum-mechanical case. Indeed, μ_{31} enters the first equation in the system (11) multiplied by μ_{23}, whereas μ_{21} is multiplied by $\mu_{33} \gg \mu_{23}$. Thus the first term prevails over the second one, and this equation is fulfilled approximately for $A^{s,a}_{212} \approx 0$.

Similarly to the quantum-mechanical case, the short-wavelength (high energy) BIC can be observed for $L_{\mathrm{BIC}} \to 0$. The two-mode approximation cannot capture this phenomenon, whereas the three-mode model works pretty well and provides not only qualitative but also fine quantitative agreement with the exact result (Fig. 8). The electric field distribution of the BIC coincides with any given accuracy with the distribution calculated in the scattering problem, if one sets parameters close enough to the BIC. Figure 9 depicts the electric field energy distribution corresponding to the scattering problem in the structure with $H = 3h$, $w = 1.2h$, $n_w = 1.84$, and $L_{\mathrm{BIC}} = 0.3h$. The incident electric field is normalized to provide unity maximum electric field energy along the structure. In the considered example, the wavelength of BIC, $\lambda_{\mathrm{BIC}} \approx 3.707h$, is an order of magnitude greater than the corresponding length of the resonator L_{BIC}.

In practice, due to imperfections of the system, material loss, and some other external perturbations, BICs are revealed as quasi-BICs with high but limited Q factor [5]. It should be noted that the qualitative physical picture of multimode interference providing BIC formation is universal and, in particular, can be applied to the description of quasi-BICs as well. However, the particular definition of interfering modes and intermode states has to be chosen appropriately, which deserves a separate study in each case.

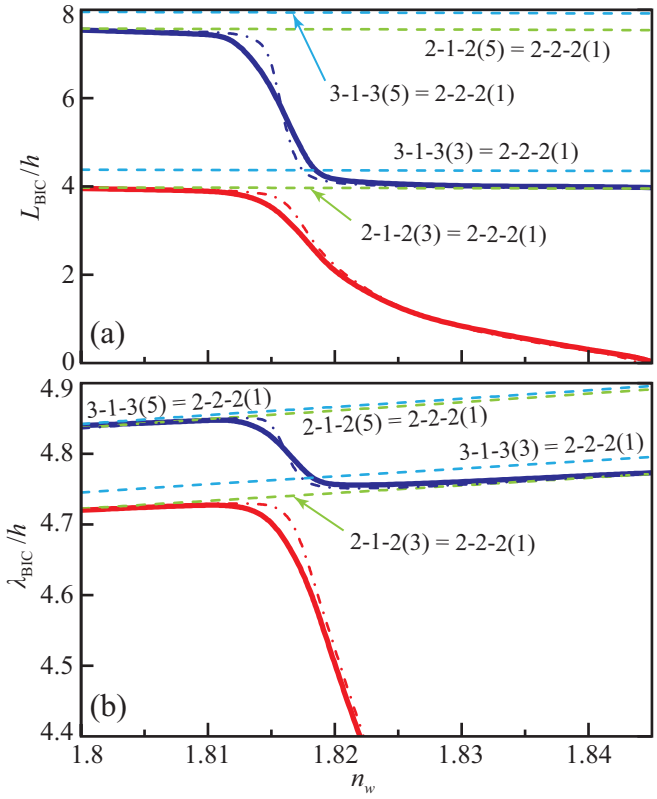

FIG. 8. Dependence of the resonator length L_{BIC} (a) and wavelength λ_{BIC} (b) of exact BICs on the dielectric constant of the impurity n_w (blue and red thick solid lines) and comparison with estimation for two-mode (dashed lines) and three-mode (dot-dashed lines) approximations. Parameters are set to $H = 3h$ and $w = 1.2h$. It is not shown in the scale of (b), but the wavelength λ_{BIC} of the short-wavelength (high energy) BIC [red line in (b)] goes down to the threshold of the second mode in WG, which is approximately $3.588h$, as the corresponding resonator length L_{BIC} tends to zero at $n_w \approx 1.845$.

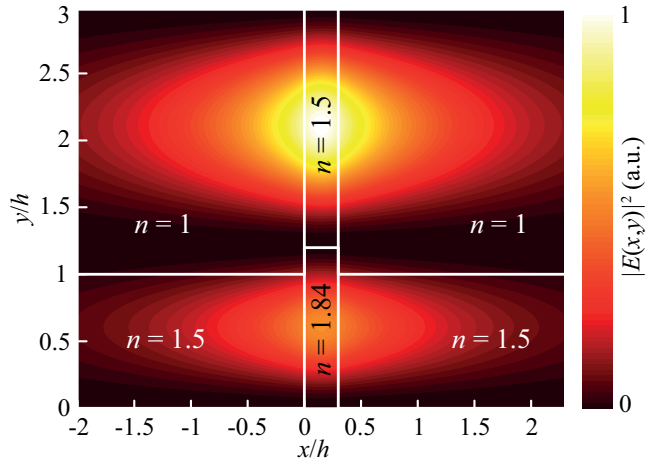

FIG. 9. Electric field energy distribution in a system with $H = 3h$, $w = 1.2h$, and $n_w = 1.84$ corresponding to a BIC at wavelength $\lambda_{BIC} \approx 3.707h$ and resonator length $L_{BIC} = 0.3h$.

V. CONCLUSION

In this paper, we took a step beyond the model proposed by Friedrich and Wintgen (the FW model), which is widely used to describe bound states in the continuum (BICs) in a variety of systems demonstrating wave interference phenomena. The original FW model describes BIC formation due to the interference of waves scattered by two localized bound states that can be, e.g., eigenmodes of the quantum-mechanical or electromagnetic cavity. However, many BICs which are found by numerical multimode simulations do not fit the FW model description and can be considered as accidental. Here, we showed that at least some such BICs can be consistently described as a result of three-mode interference. We presented a general N-mode theory of BIC formation ($N = 2$ corresponds to the FW model) in symmetric waveguide systems. We showed that for $N > 2$ the analytic form of the BIC formation condition significantly differs from that in the FW model and explicitly depends on the mode-mixing matrix elements, whose values determine how many and what particular modes should be taken into account. Finding the very location of a BIC in the parameter space of a system is a cumbersome multiparametric problem depending not only on mode-mixing matrix elements but also on mode thresholds.

The essential feature of our treatment is that we consider cavities with their localized modes being strongly hybridized by the propagating states in attached waveguides. Transport properties in the case of weak hybridization are generally formulated in terms of bound states (eigenfrequencies) of a closed resonator and coupling parameters (as in the standard FW model), which jointly determine system resonances. In the case of strong hybridization, as we discuss, the situation is more complicated, but it can be described in terms of some composite bound states also. Such composite bound states are formed by the potentials that are assembled from parts (different mode thresholds) of both the resonator and the waveguides (intermode bound states). The derived three-mode approximation coincides with the previously known two-mode model when parameters are suitable for the corresponding two-mode approximation. On the other hand, it provides a BIC description beyond two modes where a good agreement with an exact solution takes place, as we have shown by numerical simulations of both quantum-mechanical and optical examples. In particular, in this paper, we demonstrated that the three-mode model correctly describes the continuous transition in the parameter space between two FW-like BICs.

Our analytical multimode model of BIC formation is developed for quantum-mechanical WGs. However, because it is based on general properties of wave interference, its predictions are quite universal. As we show, one can expect that they will be valid also for electromagnetic waveguides, which possess a significant difference from quantum-mechanical waveguides due to the absence of true bound states in 2D systems. Our numerical simulations of electromagnetic waveguides confirm this expectation. We verify the existence therein of the aforementioned BIC transition as well as recently proposed (in quantum-mechanical WGs) subwavelength BICs due to multimode (i.e., three-mode) interference [61].

ACKNOWLEDGMENT

We would like to acknowledge the Russian Science Foundation for support under Project No. 21-19-00808.

APPENDIX: BOUND STATE IN THE CONTINUUM IN THE FOUR-MODE APPROXIMATION

For $N = 4$, BIC conditions (9) take the form [one among $N(N-1)/2 = 6$ equivalent variants]

$$\begin{aligned}\Delta^{s,a}_{1,1} &= \mu_{44}A^{s,a}_{444}\left(\mu_{22}\mu_{33}A^{s,a}_{222}A^{s,a}_{333} - \mu_{23}\mu_{32}A^{s,a}_{232}A^{s,a}_{323}\right)\\ &+ \mu_{24}A^{s,a}_{242}\left(\mu_{32}\mu_{43}A^{s,a}_{323}A^{s,a}_{434} - \mu_{42}\mu_{33}A^{s,a}_{333}A^{s,a}_{424}\right) + \mu_{34}A^{s,a}_{343}\left(\mu_{42}\mu_{23}A^{s,a}_{232}A^{s,a}_{424} - \mu_{22}\mu_{43}A^{s,a}_{222}A^{s,a}_{434}\right) = 0,\\ \Delta^{s,a}_{2,1} &= \mu_{44}A^{s,a}_{444}\left(\mu_{21}\mu_{33}A^{s,a}_{212}A^{s,a}_{333} - \mu_{31}\mu_{23}A^{s,a}_{232}A^{s,a}_{313}\right)\\ &+ \mu_{24}A^{s,a}_{242}\left(\mu_{31}\mu_{43}A^{s,a}_{313}A^{s,a}_{434} - \mu_{41}\mu_{33}A^{s,a}_{333}A^{s,a}_{414}\right) + \mu_{34}A^{s,a}_{343}\left(\mu_{41}\mu_{23}A^{s,a}_{232}A^{s,a}_{414} - \mu_{21}\mu_{43}A^{s,a}_{212}A^{s,a}_{434}\right) = 0. \end{aligned} \tag{A1}$$

From these conditions, one may expect the simplest BIC to take place if $A^{s,a}_{242} = A^{s,a}_{343} = A^{s,a}_{444} = 0$, which again is not possible. A straightforward, theoretically possible BIC requires the degeneracy of four intermode states (e.g., 2-1-2, 2-2-2, 2-3-2, and 2-4-2) and thus can hardly be achieved in any particular system. The first terms in Eqs. (A1) are exactly the same as the conditions for BIC formation in the three-mode case (11). Therefore it is expected that a specific BIC defined by conditions (11) with all nonzero $A^{s,a}_{mnm}$ will survive and be just shifted a little in the energy-parameter space with the fourth modes being taken into account if the second and third terms in Eqs. (A1) are small enough to be treated as a perturbation. Unfortunately, additional terms in Eqs. (A1) are not necessarily small and in typical systems can be of the same order as the first terms. Thus the behavior of such a BIC (and even its presence or absence) becomes very complicated with more modes taken into account, and it depends strongly on the particular parameters of the system considered.

The key conclusion that we make from conditions (A1) or their equivalent variants is the following. The two-mode approximation (10) can be generalized and require degeneracy of any intermode bound states *m-n-m* and *p-q-p* instead of 2-1-2 and 2-2-2. Indeed, suppose that μ_{mn} and μ_{pq} dominate over all the other mode-mixing matrix elements. Then, conditions (A1) can be fulfilled as soon as Eq. (12) holds true. The same result can be obtained if one considers in the same manner any finite-mode approximation (with $N > 4$).

[1] J. von Neuman and E. Wigner, Über merkwrdige diskrete Eigenwerte, Phys. Z. **30**, 465 (1929).

[2] C. W. Hsu, B. Zhen, A. D. Stone, J. D. Joannopoulos, and M. Soljačić, Bound states in the continuum, Nat. Rev. Mater. **1**, 16048 (2016).

[3] K. Koshelev, G. Favraud, A. Bogdanov, Y. Kivshar, and A. Fratalocchi, Nonradiating photonics with resonant dielectric nanostructures, Nanophotonics **8**, 725 (2019).

[4] A. Krasnok, D. Baranov, H. Li, M.-A. Miri, F. Monticone, and A. Alú, Anomalies in light scattering, Adv. Opt. Photonics **11**, 892 (2019).

[5] S. I. Azzam and A. V. Kildishev, Photonic bound states in the continuum: From basics to applications, Adv. Opt. Mater. **9**, 2001469 (2021).

[6] A. F. Sadreev, Interference traps waves in open system: Bound states in the continuum, Rep. Prog. Phys. **84**, 055901 (2021).

[7] N. M. Shubin, A. V. Friman, V. V. Kapaev, and A. A. Gorbatsevich, Bound states in the continuum in asymmetrical quantum-mechanical and electromagnetic waveguides, Phys. Rev. B **104**, 125414 (2021).

[8] C. S. Kim, A. M. Satanin, Y. S. Joe, and R. M. Cosby, Resonant tunneling in a quantum waveguide: Effect of a finite-size attractive impurity, Phys. Rev. B **60**, 10962 (1999).

[9] C. S. Kim and A. M. Satanin, Tunneling through discrete levels in the continuum, J. Exp. Theor. Phys. **88**, 118 (1999).

[10] A. F. Sadreev, E. N. Bulgakov, and I. Rotter, Bound states in the continuum in open quantum billiards with a variable shape, Phys. Rev. B **73**, 235342 (2006).

[11] Z. Yu, X. Xi, J. Ma, H. K. Tsang, C.-L. Zou, and X. Sun, Photonic integrated circuits with bound states in the continuum, Optica **6**, 1342 (2019).

[12] E. A. Bezus, D. A. Bykov, and L. L. Doskolovich, Bound states in the continuum and high-Q resonances supported by a dielectric ridge on a slab waveguide, Photonics Res. **6**, 1084 (2018).

[13] A. Kodigala, T. Lepetit, Q. Gu, B. Bahari, Y. Fainman, and B. Kanté, Lasing action from photonic bound states in continuum, Nature (London) **541**, 196 (2017).

[14] F. Yesilkoy, E. R. Arvelo, Y. Jahani, M. Liu, A. Tittl, V. Cevher, Y. Kivshar, and H. Altug, Ultrasensitive hyperspectral imaging and biodetection enabled by dielectric metasurfaces, Nat. Photonics **13**, 390 (2019).

[15] P. S. Pankin, B.-R. Wu, J.-H. Yang, K.-P. Chen, I. V. Timofeev, and A. F. Sadreev, One-dimensional photonic bound states in the continuum, Commun. Phys. **3**, 91 (2020).

[16] H. M. Doeleman, F. Monticone, W. den Hollander, A. Alù, and A. F. Koenderink, Experimental observation of a polarization vortex at an optical bound state in the continuum, Nat. Photonics **12**, 397 (2018).

[17] F. Wu, M. Luo, J. Wu, C. Fan, X. Qi, Y. Jian, D. Liu, S. Xiao, G. Chen, H. Jiang, Y. Sun, and H. Chen, Dual quasibound states in the continuum in compound grating waveguide structures for

large positive and negative Goos-Hänchen shifts with perfect reflection, Phys. Rev. A **104**, 023518 (2021).
[18] F. Wu, C. Fan, K. Zhu, J. Wu, X. Qi, Y. Sun, S. Xiao, H. Jiang, and H. Chen, Tailoring electromagnetic responses in a coupled-grating system with combined modulation of near-field and far-field couplings, Phys. Rev. B **105**, 245417 (2022).
[19] A. S. Kupriianov, Y. Xu, A. Sayanskiy, V. Dmitriev, Y. S. Kivshar, and V. R. Tuz, Metasurface Engineering through Bound States in the Continuum, Phys. Rev. Appl. **12**, 014024 (2019).
[20] D. R. Abujetas, N. van Hoof, S. ter Huurne, J. G. Rivas, and J. A. Sánchez-Gil, Spectral and temporal evidence of robust photonic bound states in the continuum on terahertz metasurfaces, Optica **6**, 996 (2019).
[21] D. Evans and R. Porter, Trapped modes embedded in the continuous spectrum, Q. J. Mech. Appl. Math. **51**, 263 (1998).
[22] C. Linton, M. McIver, P. McIver, K. Ratcliffe, and J. Zhang, Trapped modes for off-centre structures in guides, Wave Motion **36**, 67 (2002).
[23] S. Mizuno, Fano resonances and bound states in the continuum in a simple phononic system, Appl. Phys. Express **12**, 035504 (2019).
[24] A. Lyapina, A. Pilipchuk, and A. Sadreev, Bound states with orbital angular momentum in the continuum of cylindrical non-axisymmetric waveguide, Ann. Phys. (Amsterdam) **396**, 56 (2018).
[25] J. M. Zhang, D. Braak, and M. Kollar, Bound States in the Continuum Realized in the One-Dimensional Two-Particle Hubbard Model with an Impurity, Phys. Rev. Lett. **109**, 116405 (2012).
[26] S. Longhi and G. D. Valle, Tamm–Hubbard surface states in the continuum, J. Phys.: Condens. Matter **25**, 235601 (2013).
[27] A. F. Sadreev and T. V. Babushkina, Two-electron bound states in a continuum in quantum dots, JETP Lett. **88**, 312 (2008).
[28] M. A. Sierra, M. Saiz-Bretín, F. Domínguez-Adame, and D. Sánchez, Interactions and thermoelectric effects in a parallel-coupled double quantum dot, Phys. Rev. B **93**, 235452 (2016).
[29] S. V. Aksenov and M. Y. Kagan, Collapse of the Fano resonance caused by the nonlocality of the Majorana state, JETP Lett. **111**, 286 (2020).
[30] N. Shubin, A. Emelianov, Y. Uspenskii, and A. Gorbatsevich, Interacting resonances and antiresonances in conjugated hydrocarbons: exceptional points and bound states in the continuum, Phys. Chem. Chem. Phys. **23**, 20854 (2021).
[31] M. G. Silveirinha, Trapping light in open plasmonic nanostructures, Phys. Rev. A **89**, 023813 (2014).
[32] K. Koshelev, S. Lepeshov, M. Liu, A. Bogdanov, and Y. Kivshar, Asymmetric Metasurfaces with High-Q Resonances Governed by Bound States in the Continuum, Phys. Rev. Lett. **121**, 193903 (2018).
[33] E. N. Bulgakov and A. F. Sadreev, High-Q resonant modes in a finite array of dielectric particles, Phys. Rev. A **99**, 033851 (2019).
[34] H. Feshbach, Unified theory of nuclear reactions, Ann. Phys. (Amsterdam) **5**, 357 (1958).
[35] I. Rotter and J. P. Bird, A review of progress in the physics of open quantum systems: theory and experiment, Rep. Prog. Phys. **78**, 114001 (2015).
[36] N. Hatano, K. Sasada, H. Nakamura, and T. Petrosky, Some properties of the resonant state in quantum mechanics and its computation, Prog. Theor. Phys. **119**, 187 (2008).
[37] C. Blanchard, J.-P. Hugonin, and C. Sauvan, Fano resonances in photonic crystal slabs near optical bound states in the continuum, Phys. Rev. B **94**, 155303 (2016).
[38] A. A. Gorbatsevich and N. M. Shubin, Unified theory of resonances and bound states in the continuum in Hermitian tight-binding models, Phys. Rev. B **96**, 205441 (2017).
[39] A. Mostafazadeh, Pseudo-Hermiticity versus PT symmetry: The necessary condition for the reality of the spectrum of a non-Hermitian Hamiltonian, J. Math. Phys. **43**, 205 (2002).
[40] A. Mostafazadeh, Pseudo-Hermiticity and generalized PT- and CPT-symmetries, J. Math. Phys. **44**, 974 (2003).
[41] C. M. Bender and S. Boettcher, Real Spectra in Non-Hermitian Hamiltonians Having $\mathcal{PT}$ Symmetry, Phys. Rev. Lett. **80**, 5243 (1998).
[42] C. M. Bender, Making sense of non-Hermitian Hamiltonians, Rep. Prog. Phys. **70**, 947 (2007).
[43] T. Kato, *Perturbation Theory for Linear Operators*, Classics in Mathematics (Springer-Verlag, Berlin, 1995).
[44] J. Wiersig, Enhancing the Sensitivity of Frequency and Energy Splitting Detection by Using Exceptional Points: Application to Microcavity Sensors for Single-Particle Detection, Phys. Rev. Lett. **112**, 203901 (2014).
[45] J. Wiersig, Review of exceptional point-based sensors, Photonics Res. **8**, 1457 (2020).
[46] W. Chen, Ş. K. Özdemir, G. Zhao, J. Wiersig, and L. Yang, Exceptional points enhance sensing in an optical microcavity, Nature (London) **548**, 192 (2017).
[47] A. Gorbatsevich and N. Shubin, Coalescence of resonances in dissipationless resonant tunneling structures and $\mathcal{PT}$-symmetry breaking, Ann. Phys. (Amsterdam) **376**, 353 (2017).
[48] A. A. Gorbatsevich, M. N. Zhuravlev, and V. V. Kapaev, Collapse of resonances in semiconductor heterostructures as a transition with symmetry breaking in an open quantum system, J. Exp. Theor. Phys. **107**, 288 (2008).
[49] C. Ferise, P. del Hougne, S. Félix, V. Pagneux, and M. Davy, Exceptional Points of PT-Symmetric Reflectionless States in Complex Scattering Systems, Phys. Rev. Lett. **128**, 203904 (2022).
[50] S. Klaiman and N. Moiseyev, The absolute position of a resonance peak, J. Phys. B: At. Mol. Opt. Phys. **43**, 185205 (2010).
[51] H. Friedrich and D. Wintgen, Interfering resonances and bound states in the continuum, Phys. Rev. A **32**, 3231 (1985).
[52] K. Pichugin, H. Schanz, and P. Seba, Effective coupling for open billiards, Phys. Rev. E **64**, 056227 (2001).
[53] G. Cattapan and P. Lotti, Fano resonances in stubbed quantum waveguides with impurities, Eur. Phys. J. B **60**, 51 (2007).
[54] H. Kogelnik and C. V. Shank, Coupled-wave theory of distributed feedback lasers, J. Appl. Phys. **43**, 2327 (1972).
[55] R. Kazarinov and C. Henry, Second-order distributed feedback lasers with mode selection provided by first-order radiation losses, IEEE J. Quantum Electron. **21**, 144 (1985).
[56] K. Sakai, E. Miyai, and S. Noda, Coupled-wave model for square-lattice two-dimensional photonic crystal with transverse-electric-like mode, Appl. Phys. Lett. **89**, 021101 (2006).

[57] Y. Liang, C. Peng, K. Sakai, S. Iwahashi, and S. Noda, Three-dimensional coupled-wave model for square-lattice photonic crystal lasers with transverse electric polarization: A general approach, Phys. Rev. B **84**, 195119 (2011).

[58] Y. Yang, C. Peng, Y. Liang, Z. Li, and S. Noda, Analytical Perspective for Bound States in the Continuum in Photonic Crystal Slabs, Phys. Rev. Lett. **113**, 037401 (2014).

[59] U. Fano, Effects of Configuration Interaction on Intensities and Phase Shifts, Phys. Rev. **124**, 1866 (1961).

[60] X. Gao, C. W. Hsu, B. Zhen, X. Lin, J. D. Joannopoulos, M. Soljačić, and H. Chen, Formation mechanism of guided resonances and bound states in the continuum in photonic crystal slabs, Sci. Rep. **6**, 31908 (2016).

[61] N. Shubin, V. Kapaev, and A. Gorbatsevich, Bound states in the continuum in quantum-mechanical waveguide with subwavelength resonator, JETP Lett. **116**, 206 (2022).

[62] B. Zhen, C. W. Hsu, L. Lu, A. D. Stone, and M. Soljačić, Topological Nature of Optical Bound States in the Continuum, Phys. Rev. Lett. **113**, 257401 (2014).

[63] A. Pilipchuk and A. Sadreev, Accidental bound states in the continuum in an open Sinai billiard, Phys. Lett. A **381**, 720 (2017).

[64] M. S. Sidorenko, O. N. Sergaeva, Z. F. Sadrieva, C. Roques-Carmes, P. S. Muraev, D. N. Maksimov, and A. A. Bogdanov, Observation of an Accidental Bound State in the Continuum in a Chain of Dielectric Disks, Phys. Rev. Appl. **15**, 034041 (2021).

[65] G. N. Henderson, T. K. Gaylord, and E. N. Glytsis, Ballistic electron transport in semiconductor heterostructures and its analogies in electromagnetic propagation in general dielectrics, Proc. IEEE **79**, 1643 (1991).

[66] M. Asada, Y. Miyamoto, and Y. Suematsu, Gain and the threshold of three-dimensional quantum-box lasers, IEEE J. Quantum Electron. **22**, 1915 (1986).

[67] J. Sanchez-Dehesa, J. A. Porto, F. Agullo-Rueda, and F. Meseguer, Electronic energy levels of quantum-well wires, J. Appl. Phys. **73**, 5027 (1993).

[68] A. A. Gorbatsevich and V. V. Kapaev, Waveguide nanoelectronics, Russ. Microelectron. **36**, 1 (2007).

[69] See Supplemental Material at http://link.aps.org/supplemental/10.1103/PhysRevB.106.125425 for the details of the numerical calculations' convergence, derivation of BIC formation conditions within the finite-mode analytical perspective, a brief description of the auxiliary Hamiltonian formalism, and comments on the derivation of the BIC formation conditions for the three-level model.

[70] Here, we use the notation (n_x, n_y) for the eigenstate of the 2D rectangular well with $n_x - 1$ nodes along the x axis and $n_y - 1$ nodes along the y axis.

[71] M. A. Nielsen and I. L. Chuang, *Quantum Computation and Quantum Information: 10th Anniversary Edition* (Cambridge University Press, Cambridge, 2010).

[72] N. M. Shubin, A. A. Gorbatsevich, and G. Y. Krasnikov, Non-Hermitian Hamiltonians and quantum transport in multi-terminal conductors, Entropy **22**, 459 (2020).

[73] M. Robnik, A simple separable Hamiltonian having bound states in the continuum, J. Phys. A: Math. Gen. **19**, 3845 (1986).

[74] A. A. Gorbatsevich, G. Y. Krasnikov, and N. M. Shubin, $\mathcal{PT}$-symmetric interference transistor, Sci. Rep. **8**, 15780 (2018).

[75] V. Sokolov and V. Zelevinsky, Collective dynamics of unstable quantum states, Ann. Phys. (Amsterdam) **216**, 323 (1992).

[76] D. Ryndyk, *Theory of Quantum Transport at Nanoscale: An Introduction*, Springer Series in Solid-State Sciences (Springer, Cham, Switzerland, 2016).

[77] V. Pavlov-Verevkin, Trapping in the coherent radiationless decay of degenerate states, Phys. Lett. A **129**, 168 (1988).

[78] F. Remacle, M. Munster, V. Pavlov-Verevkin, and M. Desouter-Lecomte, Trapping in competitive decay of degenerate states, Phys. Lett. A **145**, 265 (1990).

[79] A. S. Pilipchuk, A. A. Pilipchuk, and A. F. Sadreev, Multichannel bound states in the continuum in coaxial cylindrical waveguide, Phys. Scr. **94**, 115004 (2019).

[80] A. S. Pilipchuk, A. A. Pilipchuk, and A. F. Sadreev, Bound states in the continuum in open spherical resonator, Phys. Scr. **95**, 085002 (2020).

[81] A. Volya and V. Zelevinsky, Non-Hermitian effective Hamiltonian and continuum shell model, Phys. Rev. C **67**, 054322 (2003).

[82] J. D. Joannopoulos, S. G. Johnson, J. N. Winn, and R. D. Meade, *Photonic Crystals* (Princeton University Press, Princeton, 2011).

[83] D. Dragoman and M. Dragoman, Optical analogue structures to mesoscopic devices, Prog. Quantum Electron. **23**, 131 (1999).

[84] D. Dragoman and M. Dragoman, Optical modeling of quantum wire arrays, IEEE J. Quantum Electron. **33**, 375 (1997).